Degradation Modeling With Long-Term Memory Considering Measurement Errors

Yunfei Shao and Wujun Si

***Abstract*—With the advancement of measurement technology, the long-term memory (LTM) effect within the degradation data of many assets has recently been detected, which implies that the future degradation process highly correlates with both the current degradation status and historical degradation trajectory across a long time period. To capture the LTM effect, several LTM-integrated degradation models have been developed in the literature. In practice, degradation data are often contaminated with measurement errors, which are ignored in most existing LTM-integrated degradation studies. Without considering measurement errors, the asset degradation modeling and reliability analysis may be biased. In this article, we propose a novel LTM-integrated degradation model that quantitatively incorporates measurement errors. Both fixed-effect and random-effect scenarios of degradation growth are considered. A maximum-likelihood estimation approach is developed to estimate the parameters of the proposed model. Based on this model, asset reliability analysis and lifetime prediction are developed. Simulation studies are implemented to evaluate the performance of the proposed model. A real case study using the capacity degradation data of lithium-ion pouch cells is conducted to illustrate the superiority of the proposed model. Results demonstrate that conventional LTM-integrated degradation models, which ignore the measurement errors, significantly misestimate the uncertainty of asset lifetime.**

***Index Terms*—Degradation test, fractional Brownian motion (FBM), lifetime prediction, long memory, observational error, reliability analysis.**

NOMENCLATURE

Acronyms

AI	Artificial intelligence.
BM	Brownian motion.
BIC	Bayesian information criterion.
FBM	Fractional Brownian motion.
FFT	Fast Fourier transform.
LTM	Long-term memory.
MLE	Maximum-likelihood estimation.
MC	Monte Carlo.
PHM	Prognostics and health management.
PDF	Probability density function.
RMSE	Root-mean-square error.

Notation

K	Number of test units.
N_j	Number of degradation measurements of unit j.
$\mathbf{Y}$	Ensemble of degradation measurements.
H	Hurst parameter.
$\alpha f(\cdot\|\boldsymbol{\eta}_f)$	Trend term of asset degradation.
$\boldsymbol{\eta}_f$	Parameters of trend term function.
σ	Diffusion parameter of degradation model.
$B_H(\cdot)$	Standard fractional Brownian motion.
ϵ_{ij}	ith measurement error of jth degradation path.
d^2	Variance of measurement errors.
α_j	Random-effect parameter of degradation.
μ_α	Mean of variable α_j.
s_α^2	Variance of α_j.
$\boldsymbol{\eta}$	Vector of model parameters.
$\hat{\boldsymbol{\eta}}$	Estimator of $\boldsymbol{\eta}$.
$l(\boldsymbol{\eta}\|\mathbf{Y})$	Log-likelihood function given observed data $\mathbf{Y}$.
$\mathbf{I}(\hat{\boldsymbol{\eta}})$	Observed Fisher information matrix.
z_x	x-quantile of standard normal distribution.
y_{th}	Failure threshold value.
T_f	First passage time.

I. INTRODUCTION

DEGRADATION modeling and reliability analysis are crucial to the PHM of modern complex systems [1]–[3]. Recently, by virtue of advances in measurement technology, a long-term memory (LTM) effect has been detected in the degradation data of many assets, including turbofan engines [4], blast furnaces [5], lithium-ion batteries [6], and chemical catalysts [7]. The LTM effect (also referred to as long-range dependence or long-range persistence) is a type of non-Markovian property and refers to the fact that the increments of asset degradation are highly correlated over a long time range [7], that is, future degradation behavior not only depends on the current asset health status but also highly correlates with the entire degradation history. In addition to the performance degradation of assets, the LTM effect has also been observed in many other fields, such as finance [8], hydrology [9], and biology [10]. Due to the widespread existence and importance of LTM effects, several LTM-integrated degradation models have recently been proposed for asset degradation modeling and reliability analysis [11]–[13].

Manuscript received January 20, 2021; revised May 29, 2021 and August 28, 2021; accepted October 31, 2021. This work was supported in part by the Kansas NASA EPSCoR Research Infrastructure Development Program under Grant 80NSSC19M0042 and in part by the National Science Foundation under Award OIA-1656006 to Wichita State University. Associate Editor: M. Grottke. *(Corresponding author: Wujun Si.)*

The authors are with the Department of Industrial, Systems and Manufacturing Engineering, Wichita State University, Wichita, KS 67260 USA (e-mail: yxshao2@shockers.wichita.edu; wujun.si@wichita.edu).

Color versions of one or more figures in this article are available at https://doi.org/10.1109/TR.2021.3125958.

Digital Object Identifier 10.1109/TR.2021.3125958

In the real world, it is inevitable that most degradation data are contaminated by measurement errors due to a variety of technical limitations. The measurement error, also referred to as observational error, has been widely studied in various research fields, including psychology [14], biology [15], healthcare [16], chemistry [17], and reliability [18]. Research has shown that ignoring measurement errors can cause several serious problems. For example, in the healthcare field, Hutcheon *et al.* [16] discovered that the failure to consider measurement errors in systolic blood pressure measurement would lead to a biased correlation quantification between systolic blood pressure and the left ventricular mass index. Another example, in psychology, is that ignoring measurement errors of the response in a job satisfaction survey significantly increased the rate of drawing a false conclusion [14]. In the context of reliability analysis, Liu and Wang [18] demonstrated that ignoring measurement errors would result in an inaccurate lifetime prediction. Therefore, it is critical to incorporate the impact of measurement errors into asset degradation modeling and reliability analysis.

In the reliability literature, most existing degradation models either ignore the LTM effect or measurement error. These models can generally be classified into three groups, i.e., general path models, stochastic process models, and artificial intelligence (AI) models. For the first group, Lu and Meeker [19] incorporated measurement errors into a random-effect general path model and studied fatigue crack growth. Si *et al.* [20] developed a multivariate general path model to analyze dynamic material deformation by considering measurement errors. For more degradation studies using the general path model, one can refer to [21] and [22]. To further capture the random behavior in a degradation path, various stochastic processes have been introduced to model asset degradations, including both Markovian and non-Markovian processes. Typical Markovian processes used for degradation modeling involve the gamma process [23], [24], the inverse Gaussian process [25], [26], and the Wiener process [27], [28]. On the basis of Markovian models, some researchers have further integrated measurement errors. For example, Whitmore [29] developed a fixed-effect Wiener process model subject to measurement errors to analyze the degradation of a transistor. Ye *et al.* [1] developed a random-effect Wiener process model with measurement errors to study the degradation of light-emitting diodes. Limited research has been conducted on non-Markovian degradation modeling. For example, Zhou and Huang [30] developed an autoregressive integrated moving average model to predict the remaining useful life of lithium-ion batteries. Although these non-Markovian processes can model the memory effect among degradation up to a limited order, they are not able to capture the LTM effect across the entire degradation path. Recently, some AI methods have also been developed for degradation analysis. For example, Kim *et al.* [31] proposed a generic health index approach based on data fusion to study multisensor degradation data. Zhu *et al.* [32] developed a multiscale convolutional neural network model for asset degradation analysis and remaining useful life prediction. Wang *et al.* [33] modeled the degradation of turbo engines through a deep-learning-based data fusion approach. However, none of these methods can capture the LTM effect.

To track the LTM effect in degradation data, some researchers have adopted fractional Brownian motion (FBM) in asset degradation modeling. The memory structure of FBM is characterized by its Hurst parameter $H \in (0, 1)$ [34]. When $0.5 < H < 1$, FBM demonstrates an LTM effect and therefore has recently been employed to study LTM-integrated degradation data of different assets. For instance, Xi *et al.* [4] proposed a degradation model with LTM effect to predict the remaining useful life of turbo engines. Zhang *et al.* [35] incorporated multiple degradation modes into an FBM-based degradation model. Si *et al.* [7] considered the LTM effect in an accelerated degradation test. Zhang *et al.* [6] developed an approximate explicit probability density function (PDF) of remaining useful life based on an LTM-integrated degradation model with multiple hidden state variables. For more studies of FBM-based degradation models, one can refer to [11]–[13]. However, these LTM-integrated degradation models ignore measurement errors and therefore may result in imprecise lifetime predictions. It should be mentioned that Xi *et al.* [36], in a conference paper, considered measurement errors in an FBM-based degradation model to analyze degradation data with a variant of the sigmoid trend. However, their model parameters were estimated via an approximate multistep procedure that may lead to nonconvergent results, and the random effects among degradation data that widely exist in practice were not considered in that paper.

To overcome the aforementioned challenges, in this article we propose a novel LTM-integrated degradation model by incorporating measurement errors. Specifically, both a fixed-effect scenario and a random-effect scenario of the proposed model are developed for asset degradation analysis. An exact maximum-likelihood estimation (MLE) method is developed to estimate the model parameters. Based on the proposed model, reliability analysis and lifetime prediction are developed. Results of simulation and case studies illustrate that the conventional models, which ignore measurement errors, significantly bias the uncertainty of lifetime estimation.

The rest of this article is summarized as follows. In Section II, the novel LTM-integrated degradation model with measurement errors under both fixed-effect and random-effect scenarios is proposed, and the corresponding MLE approach for model parameter estimation is developed. In Section III, the reliability analysis based on the proposed model is developed to calculate asset life distribution. In Section IV, simulation studies under various scenarios are implemented to verify the proposed model. In Section V, a real case study using the capacity degradation data of lithium-ion pouch cells is conducted to demonstrate the superiority of the proposed model over conventional degradation models. Finally, Section VI concludes the article and outlines future research.

II. Degradation Model

We propose an LTM-integrated degradation model with measurement errors for the degradation analysis of complex systems. First, a fixed-effect scenario of the proposed model is developed in Section II-A. To capture the heterogeneity among degradation paths, a random-effect scenario of the proposed model is

developed in Section II-B. Following three model assumptions are made in this article.

1) Degradation paths demonstrate a monotonically increasing trend over time.
2) Measurement errors follow a Gaussian distribution.
3) The asset fails when its degradation level reaches a prespecified threshold value.

These assumptions have been widely made in the literature [1], [19], [20].

A. Fixed-Effect Scenario

1) Model Description: We start by considering the fixed-effect scenario, where all degradation paths are homogenous with a common trend term. Under this scenario, an FBM-based degradation model with measurement errors is proposed to capture both the LTM effect and the influence of measurement errors. Suppose there are *K* degradation paths collected from *K* degradation units, and the *j*th degradation path contains N_j degradation measurements. The proposed fixed-effect degradation model is

$$\begin{aligned} Y(t_{ij}) &= \alpha f(t_{ij}|\boldsymbol{\eta}_f) + \sigma B_H(t_{ij}) + \epsilon_{ij} \\ \epsilon_{ij} &\sim N(0, d^2),\ i \in 1, 2, \ldots N_j,\ j \in 1, 2, \ldots .K \end{aligned} \tag{1}$$

where t_{ij} is the time of the *i*th degradation measurement for the *j*th unit; $Y(t_{ij})$ is the corresponding degradation measurement at time t_{ij}; $\alpha f(\cdot|\boldsymbol{\eta}_f)$ is a monotonic trend term with parameters α and $\boldsymbol{\eta}_f$; σ is a diffusion parameter; $B_H(\cdot)$ is the standard FBM with Hurst parameter $H \in (0, 1)$; and ϵ_{ij} is the error of the *i*th degradation measurement for unit *j*, which is assumed to be normally distributed with a mean of zero and a variance of d^2.

Specifically, in model (1), FBM (i.e., $B_H(\cdot)$) is a generalized Brownian motion (BM) to capture the memory effect defined as [34]

$$\begin{aligned} B_H(t) = B_H(0) + \frac{1}{\Gamma(H+1/2)} \Bigg\{ \int_{-\infty}^{0} \Big[(t-s)^{H-1/2} \\ - (-s)^{H-1/2} \Big] dB(s) + \int_0^t (t-s)^{H-1/2} dB(s) \Bigg\} \end{aligned} \tag{2}$$

where $\Gamma(\cdot)$ is the gamma function, i.e., $\Gamma(x) = \int_0^\infty t^{x-1} e^{-t} dt$; and $B(\cdot)$ is a standard BM. FBM is a Gaussian process with a mean of zero and a covariance function as follows [37]:

$$\mathrm{Cov}\left(B_H(t), B_H(s)\right) = \frac{1}{2}\left(|t|^{2H} + |s|^{2H} - |t-s|^{2H}\right). \tag{3}$$

Furthermore, FBM satisfies the following properties [34]:

1) $B_H(0) = 0$;
2) self-similar property, i.e., $B_H(|a|t) \sim |a|^H B_H(t)$;
3) property of stationary increments, i.e., $B_H(t) - B_H(s) \sim B_H(t-s)$ for $t > s$;
4) sample paths of $B_H(t)$ are almost surely (a.s.) Hölder continuous of order less than *H* and are a.s. nowhere differentiable.

Based on the value of *H*, FBM can be classified into three categories. When $0 < H < 0.5$, the increments of FBM are negatively correlated for nonoverlapping time intervals, and the incremental process exhibits a short-term memory effect; when $H = 0.5$, FBM degenerates into conventional BM with independent increments; and when $0.5 < H < 1$, the increments are positively correlated, and the incremental process exhibits the LTM effect. Therefore, FBM with $0.5 < H < 1$ has been widely applied to analyze the degradation data with LTM effects in the reliability field [4], [6], [28].

2) Model Parameter Estimation: For the proposed model described in Section II-A1, we develop an MLE approach to estimate the model parameters $\boldsymbol{\eta} = (\boldsymbol{\eta}_f, \alpha, \sigma^2, H, d^2)^{\mathrm{T}}$, given the collection of degradation observations $\mathbf{Y} = \{\mathbf{Y}_1, \mathbf{Y}_2, \ldots, \mathbf{Y}_K\}$, where $\mathbf{Y}_j = (Y(t_{1j}), Y(t_{2j}), \ldots, Y(t_{N_j j}))^{\mathrm{T}}$ denotes the measurement collection of the *j*th degradation path. Let $\mathbf{f}_j = (f(t_{1j}|\boldsymbol{\eta}_f), f(t_{2j}|\boldsymbol{\eta}_f), \ldots, f(t_{N_j j}|\boldsymbol{\eta}_f))^{\mathrm{T}}$; $\mathbf{B}_H^j = (B_H(t_{1j}), B_H(t_{2j}), \ldots, B_H(t_{N_j j}))^{\mathrm{T}}$; and $\boldsymbol{\epsilon}_j = (\epsilon_{1j}, \epsilon_{2j}, \ldots, \epsilon_{N_j j})^{\mathrm{T}}$. A vector form of the *j*th degradation path function can be written as

$$\mathbf{Y}_j = \alpha \mathbf{f}_j + \sigma \mathbf{B}_H^j + \boldsymbol{\epsilon}_j. \tag{4}$$

Since FBM is a Gaussian process, $\mathbf{B}_H^j$ follows a multivariate Gaussian distribution, i.e., $\mathbf{B}_H^j \sim \mathrm{MVN}(\mathbf{0}, \boldsymbol{\Sigma}_j)$, where $\boldsymbol{\Sigma}_j$ is the covariance matrix that can be calculated via (3). As a result, $\mathbf{Y}_j$ follows a multivariate Gaussian distribution, i.e., $\mathbf{Y}_j \sim \mathrm{MVN}(\alpha \mathbf{f}_j, \mathbf{G}_j)$, where the (*u*,*v*)th entry of the covariance matrix $\mathbf{G}_j$ is calculated as

$$(\mathbf{G}_j)_{uv} = \begin{cases} \frac{\sigma^2}{2}\left(t_{uj}^{2H} + t_{vj}^{2H} - |t_{uj} - t_{vj}|^{2H}\right) + d^2; \text{ for } u = v \\ \frac{\sigma^2}{2}\left(t_{uj}^{2H} + t_{vj}^{2H} - |t_{uj} - t_{vj}|^{2H}\right); \text{ for } u \neq v \end{cases} \tag{5}$$

where t_{uj} and t_{vj} represent the time epochs of the *u*th and *v*th degradation measurements of the *j*th unit, respectively. Therefore, the log-likelihood function given degradation path *j* is derived as

$$\begin{aligned} l_j(\boldsymbol{\eta}|\mathbf{Y}_j) = &-\frac{N_j}{2}\ln(2\pi) - \frac{1}{2}\ln|\mathbf{G}_j| \\ &- \frac{1}{2}(\mathbf{Y}_j - \alpha\mathbf{f}_j)^{\mathrm{T}} \mathbf{G}_j^{-1} (\mathbf{Y}_j - \alpha\mathbf{f}_j). \end{aligned} \tag{6}$$

On the basis of (6), the overall log-likelihood function given the degradation data collection $\mathbf{Y}$ can be developed as

$$\begin{aligned} l(\boldsymbol{\eta}|\mathbf{Y}) = &-\ln(2\pi)\sum_{j=1}^{K}\frac{N_j}{2} - \frac{1}{2}\sum_{j=1}^{K}\ln|\mathbf{G}_j| \\ &- \frac{1}{2}\sum_{j=1}^{K}(\mathbf{Y}_j - \alpha\mathbf{f}_j)^{\mathrm{T}}\mathbf{G}_j^{-1}(\mathbf{Y}_j - \alpha\mathbf{f}_j). \end{aligned} \tag{7}$$

The parameters $\boldsymbol{\eta}$ are estimated by maximizing the overall log-likelihood function with respect to the model parameters, i.e.,

$$\widehat{\boldsymbol{\eta}} = \arg\max_{\boldsymbol{\eta}} \{l(\boldsymbol{\eta}|\mathbf{Y})\}. \tag{8}$$

In addition to the point estimation of $\boldsymbol{\eta}$, we further develop an interval estimation method so that the confidence interval of $\boldsymbol{\eta}$ can be constructed. Based on the theory of MLE, the estimator $\widehat{\boldsymbol{\eta}}$ follows an asymptotically normal distribution under a large sample size. Its covariance matrix $\mathbf{S}$ is computed as the inverse of the observed Fisher information matrix $\mathbf{I}(\widehat{\boldsymbol{\eta}})$, i.e., $\mathbf{S}=(\mathbf{I}(\widehat{\boldsymbol{\eta}}))^{-1}$, where $\mathbf{I}(\widehat{\boldsymbol{\eta}})$ can be calculated via [38]

$$\mathbf{I}\left(\widehat{\boldsymbol{\eta}}\right) = -\left.\frac{\partial^2 l\left(\boldsymbol{\eta}|\mathbf{Y}\right)}{\partial\boldsymbol{\eta}\partial\boldsymbol{\eta}^{\mathrm{T}}}\right|_{\boldsymbol{\eta}=\widehat{\boldsymbol{\eta}}}. \tag{9}$$

The square roots of the diagonal elements of the covariance matrix $\mathbf{S}$ provide the standard errors of the corresponding estimators, i.e., $se(\hat{\eta}_i)=\sqrt{s_{ii}}$, where $\hat{\eta}_i$ is the *i*th element of $\widehat{\boldsymbol{\eta}}$, and s_{mn} is the (*m*,*n*)th entry of the matrix $\mathbf{S}$. Therefore, the $100(1-\alpha)\%$ confidence interval of η_i (the *i*th element of $\boldsymbol{\eta}$) can be constructed as $(\widehat{\eta_i}-z_{1-\alpha/2}\times se(\widehat{\eta_i}),\widehat{\eta_i}+z_{1-\alpha/2}\times se(\widehat{\eta_i}))$, where z_x is the *x*-quantile of the standard normal distribution.

B. Random-Effect Scenario

1) Model Description: To further capture the heterogeneity among degradation paths of various units, a random-effect scenario of degradation model is developed in this section. In this scenario, the degradation parameter α is assumed to be random and follow a normal distribution to capture the heterogeneity. This normality assumption to model the random effects of asset degradations has been widely adopted in the literature [1], [19]. Although the normality assumption can result in a sample of negative value of α, the issue can be neglected when the standard deviation is much lower than the mean of α. The proposed random-effect LTM-integrated degradation model with measurement errors is as follows:

$$\begin{aligned} Y\left(t_{ij}\right) &= \alpha_j f\left(t_{ij}|\boldsymbol{\eta}_f\right)+\sigma B_H\left(t_{ij}\right)+\epsilon_{ij};\epsilon_{ij}\sim N\left(0,d^2\right), \\ &\alpha_j\sim N\left(\mu_\alpha,s_\alpha^2\right), i\in 1,2,3\ldots.N_j, j\in 1,2,3\ldots.K \end{aligned} \tag{10}$$

where α_j is normally distributed with a mean of μ_α and a variance of s_α^2 as a random-effect parameter in the trend term of the *j*th degradation path. Notice that when $H=0.5$, model (10) will degenerate into the conventional Wiener-process-based degradation model with measurement errors [1].

2) Model Parameter Estimation: To estimate the parameters $\boldsymbol{\eta}=(\boldsymbol{\eta}_f,\mu_\alpha,s_\alpha^2,\sigma^2,H,d^2)^{\mathrm{T}}$ of the random-effect model, an MLE approach is developed given the degradation measurements $\mathbf{Y}=\{\mathbf{Y}_1,\mathbf{Y}_2,\ldots,\mathbf{Y}_K\}$. Specifically, a vector form of $\mathbf{Y}_j$ based on model (10) can be written as

$$\mathbf{Y}_j=\alpha_j\mathbf{f}_j+\sigma\mathbf{B}_H^j+\boldsymbol{\epsilon}_j;\alpha_j\sim N\left(\mu_\alpha,s_\alpha^2\right). \tag{11}$$

As α_j follows a Gaussian distribution, $\mathbf{Y}_j$ follows a multivariate Gaussian distribution, denoted as $\mathbf{Y}_j\sim\mathrm{MVN}(\mu_\alpha\mathbf{f}_j,\mathbf{Q}_j)$, where the (*u*,*v*)th entry of the covariance matrix $\mathbf{Q}_j$ can be calculated by

$$\left(\mathbf{Q}_j\right)_{uv}=\begin{cases} f\left(t_{uj}\right)f(t_{vj})s_\alpha^2 \\ +\frac{\sigma^2}{2}\left(t_{uj}^{2H}+t_{vj}^{2H}-|t_{uj}-t_{vj}|^{2H}\right)+d^2;\ \text{for } u=v \\ f\left(t_{uj}\right)f(t_{vj})s_\alpha^2 \\ +\frac{\sigma^2}{2}\left(t_{uj}^{2H}+t_{vj}^{2H}-|t_{uj}-t_{vj}|^{2H}\right);\ \text{for } u\neq v \end{cases}. \tag{12}$$

Given the degradation observations $\mathbf{Y}$, the overall log-likelihood function is derived as

$$\begin{aligned} l\left(\boldsymbol{\eta}|\,\mathbf{Y}\right) = &-\ln(2\pi)\sum_{j=1}^{K}\frac{N_j}{2}-\frac{1}{2}\sum_{j=1}^{K}\ln|\mathbf{Q}_j| \\ &-\frac{1}{2}\sum_{j=1}^{K}\left(\mathbf{Y}_j-\mu_\alpha\mathbf{f}_j\right)^{\mathrm{T}}\mathbf{Q}_j{}^{-1}\left(\mathbf{Y}_j-\mu_\alpha\mathbf{f}_j\right). \end{aligned} \tag{13}$$

The parameters of the random-effect model can be estimated as $\widehat{\boldsymbol{\eta}}=\arg\max_{\boldsymbol{\eta}}\{l(\boldsymbol{\eta}|\mathbf{Y})\}$.

In numerous actual cases, asset degradations are measured under the same sampling scheme, i.e., all degradation paths share the same sampling time epochs. Under such a circumstance, the overall log-likelihood function (13) can be efficiently reduced. Suppose each degradation path contains *N* measurement points. Then, $\mathbf{Q}_j$ and $\mathbf{f}_j$will be identical across different units so that the subscript *j* can be removed. Therefore, the log-likelihood function in (13) can be written as

$$\begin{aligned} l\left(\boldsymbol{\eta}|\,\mathbf{Y}\right) = &-\frac{KN}{2}\ln(2\pi)-\frac{K}{2}\ln|\mathbf{Q}| \\ &-\frac{1}{2}\sum_{j=1}^{K}\left(\mathbf{Y}_j-\mu_\alpha\mathbf{f}\right)^{\mathrm{T}}\mathbf{Q}^{-1}\left(\mathbf{Y}_j-\mu_\alpha\mathbf{f}\right). \end{aligned} \tag{14}$$

Based on (14), we calculate the partial derivatives of $l(\boldsymbol{\eta}|\mathbf{Y})$ with respect to parameters μ_α and s_α^2, and set them to zero. Therefore, the estimators of parameters μ_α and s_α^2 are derived and summarized in Proposition 1. The proof of Proposition 1 is provided in Appendix A.

Proposition 1: The MLE estimators of parameters μ_α and s_α^2 are as follows:

$$\widehat{\mu_\alpha}=\frac{\sum_{j=1}^{K}\mathbf{Y}_j^{\mathrm{T}}\mathbf{C}^{-1}\mathbf{f}}{K\mathbf{f}^{\mathrm{T}}\mathbf{C}^{-1}\mathbf{f}} \tag{15}$$

$$\widehat{s_\alpha^2}=-\frac{1}{\mathbf{f}^{\mathrm{T}}\mathbf{C}^{-1}\mathbf{f}}+\frac{\sum_{j=1}^{K}\left(\mathbf{Y}_j^{\mathrm{T}}\mathbf{C}^{-1}\mathbf{f}\right)^2}{K(\mathbf{f}^{\mathrm{T}}\mathbf{C}^{-1}\mathbf{f})^2}-\frac{\left(\sum_{j=1}^{K}\mathbf{Y}_j^{\mathrm{T}}\mathbf{C}^{-1}\mathbf{f}\right)^2}{(K\mathbf{f}^{\mathrm{T}}\mathbf{C}^{-1}\mathbf{f})^2} \tag{16}$$

where the (*u*,*v*)th entry of matrix $\mathbf{C}$ is

$$\left(\mathbf{C}\right)_{uv}=\begin{cases} \frac{\sigma^2}{2}\left(t_u^{2H}+t_v^{2H}-|t_u-t_v|^{2H}\right)+d^2;\ \text{for } u=v \\ \frac{\sigma^2}{2}\left(t_u^{2H}+t_v^{2H}-|t_u-t_v|^{2H}\right);\ \text{for } u\neq v \end{cases} \tag{17}$$

where t_u and t_v are the time epochs of the *u*th and *v*th degradation measurements shared by all degradation paths when all units

adopt the same sampling scheme, respectively, i.e., $t_u = t_{u1} = t_{u2} \ldots = t_{uK}$ and $t_v = t_{v1} = t_{v2} \ldots = t_{vK}$.

Let $\boldsymbol{\eta}^* = (\boldsymbol{\eta}_f, H, \sigma^2, d^2)^{\mathrm{T}}$ be the collection of other model parameters. By substituting $\widehat{\mu_\alpha}$ and $\widehat{s_\alpha^2}$ into (14), the reduced log-likelihood function is obtained as

$$l\left(\boldsymbol{\eta}^* | \mathbf{Y}\right) = -\frac{1}{2}K - \frac{KN}{2}\ln\left(2\pi\right) - \frac{K}{2}\ln|\mathbf{C}| - \frac{K}{2}\ln\left(\frac{K\sum_{j=1}^{K}\left(\mathbf{f}^{\mathrm{T}}\mathbf{C}^{-1}\mathbf{Y}_j\right)^2 - \left(\sum_{j=1}^{K}\mathbf{Y}_j^{\mathrm{T}}\mathbf{C}^{-1}\mathbf{f}\right)^2}{K^2\left(\mathbf{f}^{\mathrm{T}}\mathbf{C}^{-1}\mathbf{f}\right)}\right) - \frac{1}{2}\sum_{j=1}^{K}\mathbf{Y}_j^{\mathrm{T}}\mathbf{C}^{-1}\mathbf{Y}_j + \frac{\sum_{j=1}^{K}\left(\mathbf{Y}_j^{\mathrm{T}}\mathbf{C}^{-1}\mathbf{f}\right)^2}{2\mathbf{f}^{\mathrm{T}}\mathbf{C}^{-1}\mathbf{f}}. \quad (18)$$

In (18), the reduced log-likelihood is a function of parameters $\boldsymbol{\eta}^*$, which can be estimated as $\widehat{\boldsymbol{\eta}^*} = \arg\max_{\boldsymbol{\eta}^*}\{l(\boldsymbol{\eta}^*|\mathbf{Y})\}$. Subsequently, μ_α and s_α^2 can be calculated by substituting the estimated parameters $\widehat{\boldsymbol{\eta}^*} = (\widehat{\boldsymbol{\eta}_f}, \widehat{H}, \widehat{\sigma^2}, \widehat{d^2})^{\mathrm{T}}$ into (15) and (16), respectively.

To obtain an interval estimation of $\boldsymbol{\eta}^*$, the standard errors of parameters $\widehat{\boldsymbol{\eta}}_f$, $\widehat{H}$, $\widehat{\sigma^2}$, and $\widehat{d^2}$ are calculated from the inverse of the Fisher information matrix with respect to the log-likelihood function (18). Subsequently, the standard errors of $\widehat{\mu_\alpha}$ and $\widehat{s_\alpha^2}$ are calculated based on (15) and (16) using the Delta rule [38], which are summarized as

$$se\left(\hat{\mu}_\alpha\right) = \mathrm{sqrt}\left(\begin{array}{l}\left(W_1 se\left(\widehat{\sigma^2}\right)\right)^2 + \left(W_2 se\left(\widehat{H}\right)\right)^2 \\ + \left(W_3 se\left(\widehat{d^2}\right)\right)^2 + \left(\frac{\partial\hat{\mu}_\alpha}{\partial\eta_{f1}} se\left(\widehat{\eta_{f1}}\right)\right)^2 \\ + \left(\frac{\partial\hat{\mu}_\alpha}{\partial\eta_{f2}} se\left(\widehat{\eta_{f2}}\right)\right)^2 + \cdots + \left(\frac{\partial\hat{\mu}_\alpha}{\partial\eta_{fn}} se\left(\widehat{\eta_{fn}}\right)\right)^2\end{array}\right) \quad (19)$$

$$se\left(\widehat{s_\alpha^2}\right) = \mathrm{sqrt}\left(\begin{array}{l}\left(W_4 se\left(\widehat{\sigma^2}\right)\right)^2 + \left(W_5 se\left(\widehat{H}\right)\right)^2 \\ + \left(W_6 se\left(\widehat{d^2}\right)\right)^2 + \left(\frac{\partial\widehat{s_\alpha^2}}{\partial\eta_{f1}} se\left(\widehat{\eta_{f1}}\right)\right)^2 \\ + \left(\frac{\partial\widehat{s_\alpha^2}}{\partial\eta_{f2}} se\left(\widehat{\eta_{f2}}\right)\right)^2 + \cdots + \left(\frac{\partial\widehat{s_\alpha^2}}{\partial\eta_{fn}} se\left(\widehat{\eta_{fn}}\right)\right)^2\end{array}\right) \quad (20)$$

where $\boldsymbol{\eta}_f = (\eta_{f1}, \eta_{f2}, \ldots, \eta_{fn})^{\mathrm{T}}$, and the details of W_1 – W_6 are derived and provided in Appendix B.

III. Reliability Analysis

Based on the proposed LTM-integrated degradation model with measurement errors, we develop a method of reliability analysis to obtain the asset lifetime distribution given the estimated parameters $\widehat{\boldsymbol{\eta}}$. The failure time T_f of an asset is assumed to be the first passage time when its underlying degradation level goes beyond a predetermined degradation threshold value y_{th}, i.e.,

$$T_f = \inf\left\{t | Y_u\left(t | \boldsymbol{\eta}\right) \geq y_{th}\right\} \quad (21)$$

Algorithm 1: A Monte Carlo Approach to Calculate the Asset Lifetime Distribution.

Step 1. Obtain the point estimates $\widehat{\boldsymbol{\eta}}$ of model parameters via the MLE method in Section II.

Step 2. For *j* = 1 ∼ *L*, simulate the *j*th underlying degradation path (i.e., $\mathbf{Y}_u^j$) using $\widehat{\boldsymbol{\eta}}$ (*L* is sufficiently large):

2.1 Simulate the *j*th trend term: for the fixed-effect scenario, $\alpha = \widehat{\alpha}$; for the random-effect scenario, $\widehat{\alpha_j} \sim N(\widehat{\mu_\alpha}, \widehat{s_\alpha^2})$; and $\mathbf{f}_j$ is simulated based on parameters $\widehat{\boldsymbol{\eta}_f}$.

2.2 Simulate the *j*th FBM term $\mathbf{B}_H^j$ using a fast Fourier transformation (FFT) method [39].

2.3 Obtain $\mathbf{Y}_u^j$ of the fixed-effect and random-effect scenarios, respectively, as follows: $\mathbf{Y}_u^j = \widehat{\alpha}\mathbf{f}_j + \widehat{\sigma}\mathbf{B}_{\widehat{H}}^j$ and $\mathbf{Y}_u^j = \widehat{\alpha_j}\mathbf{f}_j + \widehat{\sigma}\mathbf{B}_{\widehat{H}}^j$,

Step 3. Calculate the lifetime distribution:

3.1 For *j* = 1 ∼ *L*, calculate the *j*th failure time using (21), denoted as T_f^j.

3.2 Calculate the lifetime distribution as $F(t|\widehat{\boldsymbol{\eta}}) = L^{-1}\sum_{j=1}^{L} I_t(T_f^j)$, where $I_t\left(T_f^j\right) = \begin{cases} 1; \text{ if } T_f^j \leq t \\ 0; \text{ otherwise} \end{cases}$.

where $Y_u(t|\boldsymbol{\eta})$ is the underlying degradation level, and $Y(t|\boldsymbol{\eta}) = Y_u(t|\boldsymbol{\eta}) + \varepsilon(t)$. Due to the complexity of the proposed model, the closed-form lifetime distribution is not available in most situations. To overcome this difficulty, a Monte Carlo (MC) approach is developed to calculate the lifetime distribution. Details of the MC method are summarized in Algorithm 1.

More specifically, in Step 2.2 of Algorithm 1, the FFT method is applied to simulating $\mathbf{B}_H^j$. In the literature, there are three major approaches to simulate a path of the FBM, i.e., Hosking method [40], Cholesky method [41], and FFT method. Among them, the FFT method has the lowest computational complexity of $O(n\log(n))$ for simulating a discretized FBM of length n, whereas the computational complexity of the Hosking and Cholesky methods are $O(n^3)$ and $O(n^2)$, respectively [42].

IV. Simulation Study

To evaluate the performance of the proposed model and the corresponding MLE approach for parameter estimation, we implement simulation studies under both fixed-effect and random-effect scenarios. The fixed-effect model and the random-effect model are assessed in Section IV-A and Section IV-B, respectively.

A. Fixed-Effect Model

1) Data Simulation: For illustration purposes, a linear trend term is selected in the degradation modeling as the degradation or transformed degradation of numerous assets exhibits a linear trend [1], [29]. The degradation paths are simulated using the following fixed-effect LTM-integrated model with measurement

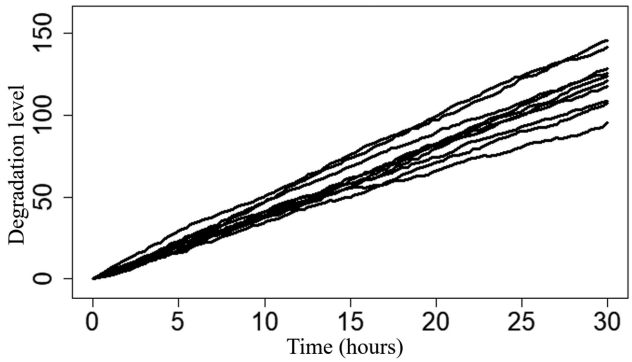

Fig. 1. Simulated degradation paths using model P_1.

TABLE I
POINT ESTIMATES AND STANDARD ERRORS OF P_1 PARAMETERS

Parameter	Point Estimate	Standard Error
H	0.809	0.0363
σ^2	0.862	0.116
α	4.04	0.152
d^2	0.107	8.69×10^{-3}

errors:

$$P_1 : Y(t) = \alpha t + \sigma B_H(t) + \epsilon; \epsilon \sim N\left(0, d^2\right). \quad (22)$$

The model parameters $\boldsymbol{\eta} = (H, \sigma^2, \alpha, d^2)^{\mathrm{T}}$ are specified as $(0.8, 1, 4, 0.1)^{\mathrm{T}}$, and the number of generated degradation paths is set at $K = 10$. Each degradation path contains $N_j = 100$ measurements that are equally spaced in a time interval $[0, 30]$. The simulated degradation paths are shown in Fig. 1.

2) Parameter Estimation: The simulated degradation paths shown in Fig. 1 are then analyzed using the fixed-effect model P_1. The model parameters $\boldsymbol{\eta}$ and corresponding standard errors are estimated through (8) and (9), which are listed in Table I. Note that the point estimates of the model parameters are close to the prespecified values, which demonstrates that the proposed MLE method performs well under the current sample size.

To further evaluate the performance of the proposed MLE method, we repeat the simulation process for $M = 1000$ times under different sample sizes, i.e., $K = 10$, 20, and 50. The root-mean-square errors (RMSEs) of the parameter estimation are calculated as $\mathrm{RMSE}(\widehat{\eta}_i) = \mathrm{sqrt}(\frac{1}{M}\sum_{l=1}^{M}(\eta_i - \widehat{\eta}_{il})^2)$, where $\widehat{\eta}_{il}$ is the estimate of parameter η_i in the lth iteration, and results are summarized in Table II. It can be observed that the RMSEs are generally small. As the sample size increases, the RMSEs of the parameter estimation all decrease, which demonstrates the efficiency of the MLE approach.

3) Model Comparison: To illustrate the advantage of the proposed fixed-effect model P_1, a model comparison is conducted between P_1 and a conventional LTM-integrated fixed-effect degradation model (P_2) that ignores measurement errors

$$P_2 : Y(t) = \alpha t + \sigma B_H(t) \quad (23)$$

where P_2 depends on three parameters $\boldsymbol{\eta} = (H, \sigma^2, \alpha)^{\mathrm{T}}$. Model P_2 is applied to study the simulated degradation data in Fig. 1.

TABLE II
RMSES OF PARAMETER ESTIMATION OF P_1 UNDER DIFFERENT SAMPLE SIZES

Sample Size (K)	10	30	50
$RMSE\left(\widehat{H}\right)$	0.0395	0.0213	0.0165
$RMSE\left(\widehat{\sigma^2}\right)$	0.132	0.0715	0.0564
$RMSE\left(\widehat{\alpha}\right)$	0.162	0.0918	0.0719
$RMSE\left(\widehat{d^2}\right)$	9.20×10^{-3}	5.16×10^{-3}	3.88×10^{-3}

TABLE III
POINT ESTIMATES AND STANDARD ERRORS OF P_2 PARAMETERS

Parameter	Point Estimate	Standard Error
H	0.526	0.0150
σ^2	1.20	0.0704
α	4.05	0.0690

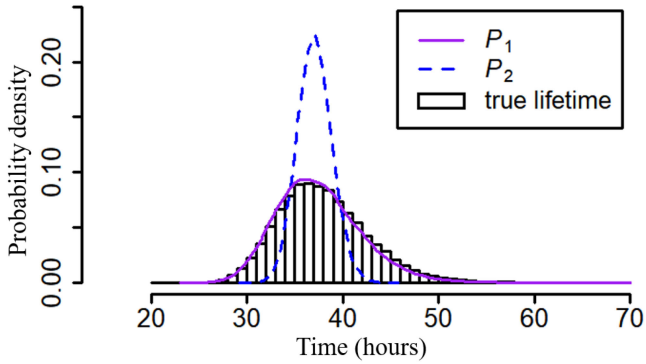

Fig. 2. PDFs of the predicted lifetime using P_1 and P_2.

Point estimates of the model parameters and corresponding standard errors are summarized in Table III.

Based on the estimated parameters of P_1 and P_2, the PDFs of the predicted lifetime using these two models are computed following Algorithm 1, where the failure threshold value is specified as $y_{th} = 150$. The predicted lifetime distributions along with a histogram of the true lifetime are presented in Fig. 2. Note that the histogram of the true lifetime is obtained based on the true/prespecified parameter values of model P_1.

In addition, the means and standard deviations of the predicted lifetime distributions of P_1 and P_2 are calculated. The means of lifetime are 37.52 and 37.07 for P_1 and P_2, respectively, and the standard deviations are 4.41 and 1.82, respectively. It can be seen that the mean values are relatively close, whereas the conventional model P_2 significantly underestimates the uncertainty of asset lifetime. Therefore, it is critical to consider measurement errors in LTM-integrated degradation modeling.

B. Random-Effect Model

1) Data Simulation: For some assets, the degradation may demonstrate heterogeneities among different units. To capture such heterogeneities, we consider a random-effect

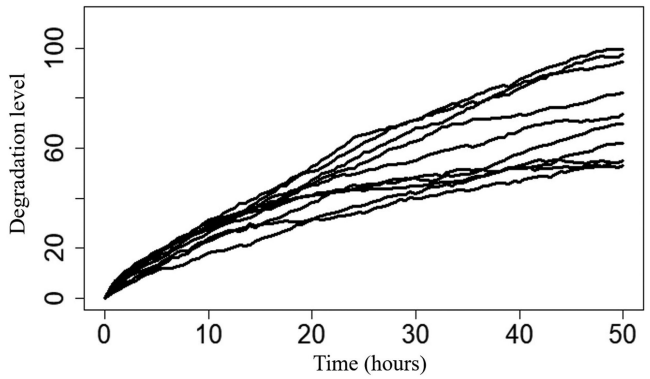

Fig. 3. Simulated degradation paths using model P_3.

TABLE IV
POINT ESTIMATES AND STANDARD ERRORS OF P_3 PARAMETERS

Parameter	Point Estimate	Standard Error
H	0.833	0.0370
σ^2	0.469	0.0652
d^2	0.0491	5.46×10^{-3}
μ_α	4.82	0.0213
s_α^2	0.671	0.105
β	0.709	0.0148

LTM-integrated degradation model with measurement errors as follows:

$$P_3 : Y(t) = \alpha t^{\beta} + \sigma B_H(t) + \epsilon; \quad \alpha \sim N\left(\mu_\alpha, s_\alpha^2\right), \epsilon \sim N\left(0, d^2\right). \tag{24}$$

Specifically, a power law trend term is employed in the degradation model, which has been widely used in the reliability literature [1], [43]. The model parameters of P_3 are $\boldsymbol{\eta} = (H, \sigma^2, d^2, \mu_\alpha, s_\alpha^2, \beta)^{\mathrm{T}}$. To simulate degradation paths using P_3, the model parameters are designated as $\boldsymbol{\eta} = (0.85, 0.5, 0.05, 5, 1, 0.7)^{\mathrm{T}}$. Based on this parameter setting, we simulate $K = 10$ degradation paths, and each path contains $N_j = 100$ measurements that are equally distributed in a time interval $[0, 50]$. The simulated degradation paths are illustrated in Fig. 3.

2) Parameter Estimation: We apply the proposed random-effect model to analyze the simulated degradation paths in Fig. 3. The model parameters $\boldsymbol{\eta}$ and the corresponding standard errors are estimated using the MLE method developed in Section II-B2, which are summarized in Table IV.

To examine the performance of the proposed MLE approach for parameter estimation, an RMSE test is also conducted under different sample sizes. We repeat the simulation process in Section IV-B1 for $M = 1000$ times, and the sample sizes are specified as $K = 10$, 30, and 50. Table V summarizes the calculated RMSEs of parameter estimates of P_3. It can be seen that the RMSEs are generally small and decrease as the sample size increases, which demonstrates a good performance of the proposed MLE approach.

TABLE V
RMSES OF PARAMETER ESTIMATION OF P_3 UNDER DIFFERENT SAMPLE SIZES

Sample Size (K)	10	30	50
$RMSE\left(\widehat{H}\right)$	0.0393	0.0229	0.0160
$RMSE\left(\widehat{\sigma^2}\right)$	0.0826	0.0531	0.0347
$RMSE\left(\widehat{d^2}\right)$	5.58×10^{-3}	3.21×10^{-3}	2.43×10^{-3}
$RMSE\left(\widehat{\mu_\alpha}\right)$	0.376	0.211	0.163
$RMSE\left(\widehat{s_\alpha^2}\right)$	0.593	0.373	0.296
$RMSE\left(\hat{\beta}\right)$	1.62×10^{-2}	9.06×10^{-3}	7.50×10^{-3}

TABLE VI
POINT ESTIMATES AND STANDARD ERRORS OF P_4 PARAMETERS

Parameter	Point Estimate	Standard Error
H	0.601	0.0182
σ^2	0.519	0.0305
μ_α	4.93	0.336
s_α^2	0.765	0.424
β	0.697	0.0111

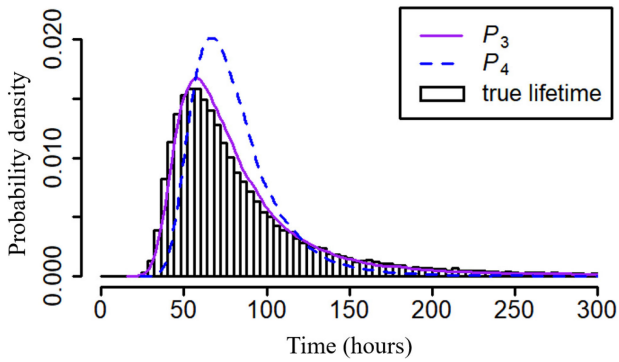

Fig. 4. Predicted lifetime distributions using P_3 and P_4.

3) Model Comparison: To demonstrate the superiority of the proposed random-effect model P_3, we compare it with an LTM-integrated random-effect model without considering the measurement errors as follows:

$$P_4 : Y(t) = \alpha t^{\beta} + \sigma B_H(t); \alpha \sim N\left(\mu_\alpha, s_\alpha^2\right) \tag{25}$$

where the parameters of model P_4 are $\boldsymbol{\eta} = (H, \sigma^2, \mu_\alpha, s_\alpha^2, \beta)^{\mathrm{T}}$. The model P_4 is applied to study the simulated degradation paths in Fig. 3. Point estimates of $\boldsymbol{\eta}$ and corresponding standard errors are computed and listed in Table VI.

On the basis of the estimated parameters of models P_3 and P_4, the lifetime distributions of both models are calculated using Algorithm 1 with a failure threshold value specified as $y_{th} = 100$. The predicted lifetime distributions along with the histogram of the true lifetime are illustrated in Fig. 4. Furthermore, we compute the means and standard deviations of the predicted

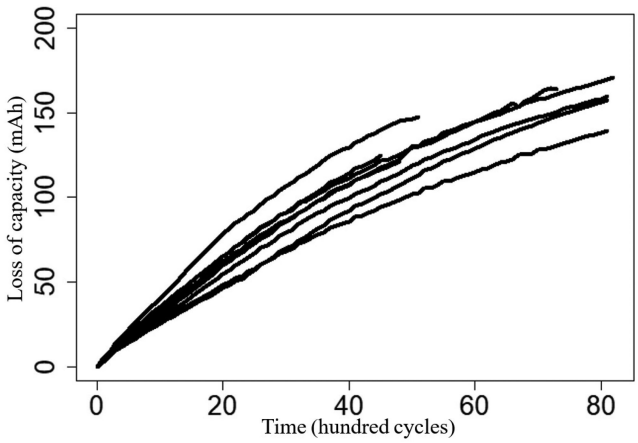

Fig. 5. Degradation paths of eight Kokam 740 mAh lithium-ion pouch cells (loss of capacity versus degradation cycle).

lifetime distributions of P_3 and P_4. The means of P_3 and P_4 are 88.63 and 83.15, respectively, and the standard deviations are 70.14 and 30.43, respectively. Similarly, results reveal that the means are relatively close for these two models, whereas the conventional model P_4, which ignores measurement errors, significantly misestimates the lifetime uncertainty. This also demonstrates the necessity of incorporating measurement errors into the LTM-integrated degradation model.

V. Case Study

To further verify the proposed model, we conduct a real case study based on the degradation data of lithium-ion pouch cells. Section V-A briefly describes the dataset, Section V-B provides the estimation results of model parameters, and Section V-C performs comparisons between the proposed model and conventional models.

A. Data Description

A publicly accessible dataset on the capacity degradation of eight Kokam 740 mAh lithium-ion pouch cells is applied to validate the performance of the proposed model [44]. The capacity degradation of these cells was measured via an aging experiment, which was conducted in a thermal chamber at 40 °C under predetermined stress cycles. Each stress cycle consisted of a constant-current-constant-voltage charging process and a discharging process based on the urban Artemis profile. The capacities of the cells were periodically measured with a time interval of 100 cycles via a pseudo open-circuit voltage discharging method (i.e., discharging cells under a current of 40 mA). Fig. 5 illustrates the eight capacity degradation paths of the cells (notice that eight outliers have been removed from the 511 measurements in total).

B. Parameter Estimation

We apply the proposed model to study the cell degradation data in Fig. 5. Since these degradation paths demonstrate an approximate power law trend, a power law function is selected to model the trend term of degradation. Therefore, the proposed models under the fixed-effect and random-effect scenarios are constructed, respectively, as follows:

$$P_5 : Y(t) = \alpha t^{\beta} + \sigma B_H(t) + \epsilon; \epsilon \sim N\left(0, d^2\right) \tag{26}$$

$$P_6 : Y(t) = \alpha t^{\beta} + \sigma B_H(t) + \epsilon;$$
$$\alpha \sim N\left(\mu_\alpha, s_\alpha^2\right), \epsilon \sim N\left(0, d^2\right). \tag{27}$$

Parameters of the fixed-effect model P_5 and random-effect model P_6 are $\boldsymbol{\eta} = (H, \sigma^2, d^2, \beta, \alpha)^{\mathrm{T}}$ and $\boldsymbol{\eta} = (H, \sigma^2, d^2, \beta, \mu_\alpha, s_\alpha^2)^{\mathrm{T}}$, respectively. Given the degradation measurements shown in Fig. 5, the parameters and corresponding standard errors of models P_5 and P_6 are calculated using the MLE approach in Sections II-A2 and II-B2, respectively, which are listed in Table VII. It can be observed from Table VII that the standard deviation of α (i.e., 0.170) is much lower than the mean value of α (i.e., 4.63) using the proposed random-effect model P_6. This justifies the normality assumption made earlier in Section II-B1. Similar observations can also be made from Table IV in the simulation study.

TABLE VII
Point Estimates and Standard Errors of P_5 and P_6 Parameters

P_5			P_6		
$\boldsymbol{\eta}$	Point Estimate	Standard Error	$\boldsymbol{\eta}$	Point Estimate	Standard Error
H	0.967	0.0179	H	0.964	0.0196
σ^2	0.451	0.205	σ^2	0.638	0.136
d^2	0.166	0.0139	d^2	0.177	0.0150
β	0.836	0.0135	β	0.839	0.0129
α	4.61	0.254	μ_α	4.63	0.254
	—		s_α^2	0.170	0.868

C. Model Comparison

To demonstrate the superiority of the proposed model, a comparison with conventional models that ignore measurement errors is conducted. The following models P_7 and P_8 denote the conventional fixed-effect and random-effect models, respectively:

$$P_7 : Y(t) = \alpha t^{\beta} + \sigma B_H(t) \tag{28}$$

$$P_8 : Y(t) = \alpha t^{\beta} + \sigma B_H(t); \alpha \sim N\left(\mu_\alpha, s_\alpha^2\right). \tag{29}$$

The model parameters of P_7 and P_8 are $\boldsymbol{\eta} = (H, \sigma^2, \beta, \alpha)^{\mathrm{T}}$ and $\boldsymbol{\eta} = (H, \sigma^2, \beta, \mu_\alpha, s_\alpha^2)^{\mathrm{T}}$, respectively. Models P_7 and P_8 are then applied to analyze the degradation data of pouch cells shown in Fig. 5. Parameters and corresponding standard errors of P_7 and P_8 are computed via the MLE approach and are summarized in Table VIII.

For reliability analysis of the pouch cells, we specify the failure threshold value as $y_{th} = 150$ mAh, i.e., the failure occurs when the loss of capacity reaches 150 mAh. Based on the estimated model parameters, the predicted lifetime distributions

TABLE VIII
POINT ESTIMATES AND STANDARD ERRORS OF P_7 AND P_8 PARAMETERS

P_7			P_8		
$\boldsymbol{\eta}$	Point Estimate	Standard Error	$\boldsymbol{\eta}$	Point Estimate	Standard Error
H	0.624	0.0212	H	0.564	0.0254
σ^2	0.574	0.0371	σ^2	0.529	0.0340
β	0.813	0.0116	β	0.812	0.0103
α	4.86	0.231	μ_α	4.94	0.286
	—		s_α^2	0.301	0.184

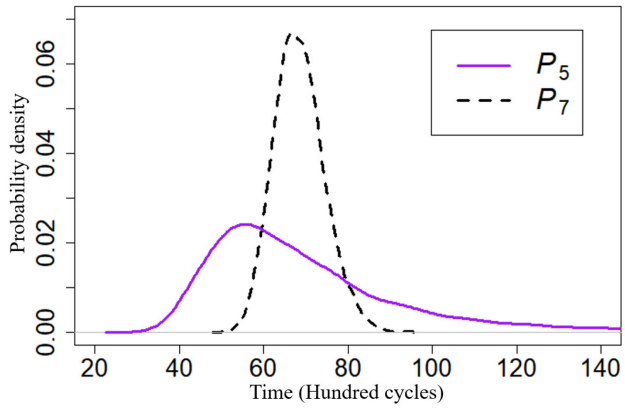

Fig. 6. PDFs of the predicted lifetime using models P_5 and P_7.

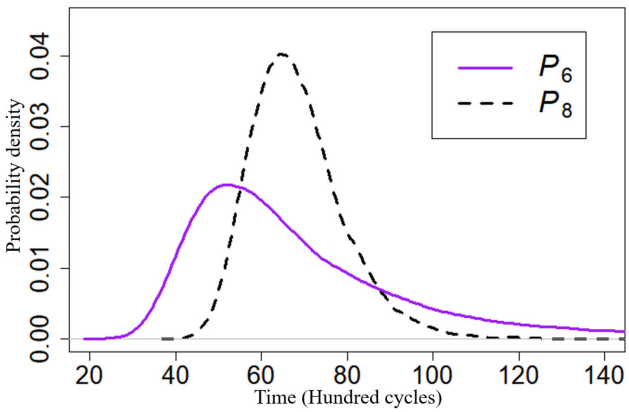

Fig. 7. PDFs of the predicted lifetime using models P_6 and P_8.

of models $P_5 - P_8$ are calculated using Algorithm 1. Figs. 6 and 7 illustrate PDFs of the predicted lifetime using the proposed model and the conventional model under the fixed-effect and random-effect scenarios, respectively. It is observed that the conventional model that ignores measurement errors significantly biases the uncertainty of the lifetime estimation under both scenarios, which is consistent with the results of simulation studies discussed in Section IV.

In addition to the conventional LTM-integrated degradation models, we further compare the proposed model with a conventional BM-based random-effect degradation model with measurement errors in [1], which does not consider the LTM effect.

TABLE IX
POINT ESTIMATES AND STANDARD ERRORS OF P_{B} PARAMETERS

Parameter	Point Estimate	Standard Error
σ^2	0.690	0.0358
d^2	0.0271	0.0212
β	0.806	0.00840
μ_α	5.06	0.270
s_α^2	0.578	0.156

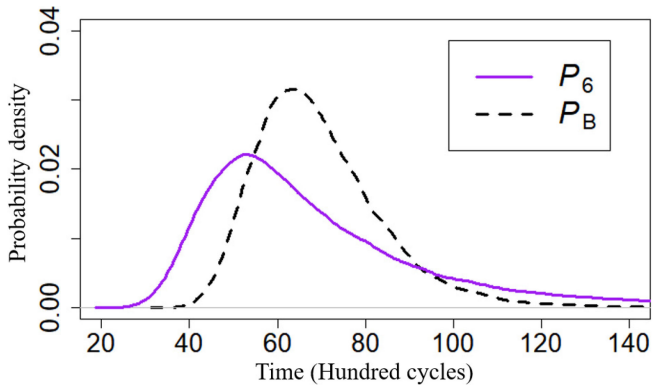

Fig. 8. PDFs of the predicted lifetime calculated by models P_6 and P_{B}.

The BM-based model is

$$P_{\mathrm{B}} : Y(t) = \alpha t^{\beta} + \sigma B(t) + \epsilon;$$
$$\alpha \sim N\left(\mu_\alpha, s_\alpha^2\right), \epsilon \sim N\left(0, d^2\right) \tag{30}$$

where $B(t)$ is the standard BM. The model parameters of P_{B} are $\boldsymbol{\eta} = (\sigma^2, d^2, \beta, \mu_\alpha, s_\alpha^2)^{\mathrm{T}}$, which are estimated using the Li-ion pouch cell degradation data in Fig. 5 by an MLE approach and summarized in Table IX.

Based on the estimated parameters of model P_{B}, the predicted lifetime distribution is computed. Fig. 8 shows PDFs of the predicted lifetime calculated by models P_6 and P_{B}. It can be observed that the conventional BM-based degradation model, P_{B}, which ignores the LTM effect, underestimates the lifetime uncertainty.

To further compare the performances of models P_5 – P_8 and P_{B}, the means of life prediction, standard deviations of life prediction, and Bayesian information criteria (BICs) are calculated and listed in Table X. It is observed that the means of these five models are relatively close, whereas the standard deviations of models P_7 and P_8 are significantly smaller than those of models P_5 and P_6, respectively. This indicates that the conventional models P_7 and P_8, without considering measurement errors, significantly underestimate the uncertainty of the lifetime estimation. Moreover, model P_{B}, which ignores the LTM effect, also significantly underestimates the life uncertainty. In addition, the proposed models have significantly smaller BICs than conventional models, which also demonstrates the superiority of the proposed models. It can be seen that the predicted lifetime distributions using models P_5 and P_6, as shown in Fig. 9, are similar, and their BICs are relatively

TABLE X
LIFE MEANS, STANDARD DEVIATIONS, AND BICS OF P_5 – P_8 AND P_B

Model Index	Mean	Standard Deviation	BIC
P_5	69.85	29.36	1071.894
P_6	69.74	35.38	1077.301
P_7	68.42	5.990	1184.579
P_8	68.18	10.68	1177.271
P_B	69.62	14.92	1182.508

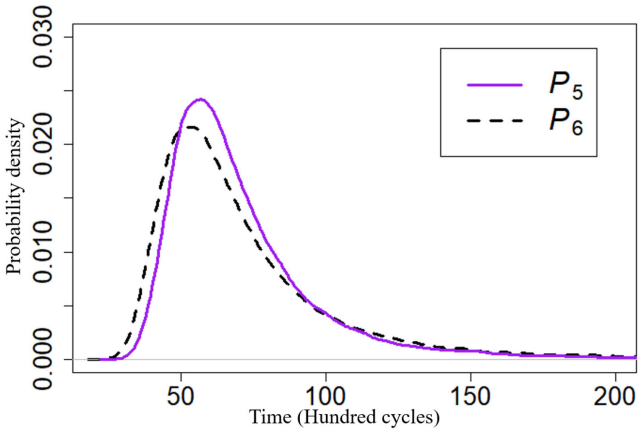

Fig. 9. PDFs of the predicted lifetime using models P_5 and P_6.

close. This indicates a similar performance between P_5 and P_6 in analyzing the capacity degradation of the lithium-ion pouch cells, that is, for the lithium-ion pouch cell data, the better fit attained by introducing heterogeneity as in model P_6 does not improve the performance in terms of BIC.

In addition, we also consider the random effect of more parameters in the proposed model. Besides the normality assumption on parameter α, parameters σ^2 and d^2 are further assumed to follow gamma distributions to guarantee the nonnegativity. This random-effect model is summarized as

$$\begin{aligned} &P_{\mathrm{R}}: Y(t) = \alpha t^{\beta} + \sigma B_H(t) + \epsilon; \\ &\alpha \sim N\left(\mu_\alpha, s_\alpha^2\right), \epsilon \sim N\left(0, d^2\right) \\ &\sigma^2 \sim \mathrm{Gamma}\left(k_{\sigma^2}, \theta_{\sigma^2}\right), d^2 \sim \mathrm{Gamma}\left(k_{d^2}, \theta_{d^2}\right) \end{aligned} \quad (31)$$

where k_{σ^2} and θ_{σ^2} are the shape and scale parameters of σ^2, respectively; k_{d^2} and θ_{d^2} are the shape and scale parameters of d^2, respectively; and the model parameters are $\boldsymbol{\eta} = (H, \beta, \mu_\alpha, s_\alpha^2, k_{\sigma^2}, \theta_{\sigma^2}, k_{d^2}, \theta_{d^2})^{\mathrm{T}}$. Based on an MLE approach, $\boldsymbol{\eta}$ is estimated and summarized in Table XI.

To compare the proposed random-effect model P_6 with model P_{R}, the BIC of model P_{R} is computed as 1081.152, which is slightly larger than the BIC of P_6 (i.e., 1077.301). Therefore, model P_6 performs slightly better than model P_{R}. This result indicates that considering the random effect of more parameters does not improve the performance of the proposed model in terms of BIC. This is due to the fact that although P_{R} is more general, it introduces several additional parameters that are penalized in the BIC.

TABLE XI
POINT ESTIMATES AND STANDARD ERRORS OF P_{R} PARAMETERS

Parameter	Point Estimate	Standard Error
H	0.895	0.0138
β	0.816	0.00727
μ_α	4.68	0.185
s_α^2	0.348	0.156
k_{σ^2}	2.74	1.42
θ_{σ^2}	0.154	0.0939
k_{d^2}	2.52	1.62
θ_{d^2}	0.110	0.0876

VI. CONCLUSION

The LTM effect has recently been detected in the degradation process of various assets. Most existing LTM-integrated degradation studies have ignored measurement errors, which may result in a biased reliability estimation and life prediction. In this article, we proposed a novel LTM-integrated degradation model by incorporating measurement errors under both fixed-effect and random-effect scenarios. An MLE method was developed for the model parameter estimation. Based on the model and estimated parameters, asset reliability analysis was developed to compute the lifetime distribution of assets. Simulation studies were implemented to evaluate the performance of the proposed model, and a real case study on the capacity degradation of lithium-ion pouch cells was conducted to validate the proposed model. Results reveal that the conventional LTM-integrated models, which neglect the measurement errors, significantly misestimate asset life uncertainty, whereas the proposed model provides more accurate life estimations.

In this article, the random effect of the trend term was considered in the degradation modeling as widely adopted in the literature. In the future, it would be an interesting topic to further consider the heterogeneity of the Hurst parameter among various degradation paths. Moreover, measurement errors are assumed to be independently and identically distributed across degradation signals in the proposed model. Another future topic would be to apply nonidentical or correlated distributions to model measurement errors.

APPENDIX

A. Proof of Proposition 1

Using the vector notation, the matrix $\mathbf{Q}$ in (14) can be written as $\mathbf{Q} = s_\alpha^2 \mathbf{f}\mathbf{f}^{\mathrm{T}} + \mathbf{C}$. We obtain the determinant of $\mathbf{Q}$ as

$$\begin{aligned} \det(\mathbf{Q}) &= \det\left(s_\alpha^2 \mathbf{f}\mathbf{f}^{\mathrm{T}} + \mathbf{C}\right) = \det\left(\mathbf{C}\left(\mathbf{I} + \mathbf{C}^{-1} s_\alpha^2 \mathbf{f}\mathbf{f}^{\mathrm{T}}\right)\right) \\ &= \det(\mathbf{C}) \det\left(\mathbf{I} + \mathbf{C}^{-1} s_\alpha^2 \mathbf{f}\mathbf{f}^{\mathrm{T}}\right). \end{aligned} \quad (32)$$

Using Sylvester's determinant theorem [45], $\det(\mathbf{Q})$ is derived as

$$\begin{aligned}\det(\mathbf{Q}) &= \det(\mathbf{C})\det\left(\mathbf{I}+\mathbf{C}^{-1}s_\alpha^2\mathbf{f}\mathbf{f}^{\mathrm{T}}\right)\\ &= \det(\mathbf{C})\left(1+s_\alpha^2\mathbf{f}^{\mathrm{T}}\mathbf{C}^{-1}\mathbf{f}\right).\end{aligned} \tag{33}$$

By applying the Sherman–Morrison formula [46], the inverse matrix of $\mathbf{Q}$ can be calculated by

$$\mathbf{Q}^{-1} = \left(s_\alpha^2\mathbf{f}\mathbf{f}^{\mathrm{T}}+\mathbf{C}\right)^{-1} = \mathbf{C}^{-1} - \frac{s_\alpha^2\mathbf{C}^{-1}\mathbf{f}\mathbf{f}^{\mathrm{T}}\mathbf{C}^{-1}}{1+s_\alpha^2\mathbf{f}^{\mathrm{T}}\mathbf{C}^{-1}\mathbf{f}}. \tag{34}$$

We then substitute (33) and (34) into (14), and the following log-likelihood function is obtained:

$$\begin{aligned}l(\boldsymbol{\eta}|\mathbf{Y}) = &-\frac{KN}{2}\ln(2\pi) - \frac{K}{2}\ln\left(\det(\mathbf{C})\left(1+s_\alpha^2\mathbf{f}^{\mathrm{T}}\mathbf{C}^{-1}\mathbf{f}\right)\right)\\ &-\frac{1}{2}\sum_{j=1}^{K}(\mathbf{Y}_j-\mu_\alpha\mathbf{f})^{\mathrm{T}}\left(\mathbf{C}^{-1}-\frac{s_\alpha^2\mathbf{C}^{-1}\mathbf{f}\mathbf{f}^{\mathrm{T}}\mathbf{C}^{-1}}{1+s_\alpha^2\mathbf{f}^{\mathrm{T}}\mathbf{C}^{-1}\mathbf{f}}\right)(\mathbf{Y}_j-\mu_\alpha\mathbf{f}).\end{aligned} \tag{35}$$

To maximize $l(\boldsymbol{\eta}|\mathbf{Y})$, we calculate its partial derivatives with respect to parameters μ_α and s_α^2, and set these two derivatives to 0. The following equations are derived:

$$\begin{aligned}\frac{\partial l(\boldsymbol{\eta}|\mathbf{Y})}{\partial\mu_\alpha} = &\sum_{j=1}^{K}\mathbf{Y}_j{}^{\mathrm{T}}\left(\mathbf{C}^{-1}-\frac{s_\alpha^2\mathbf{C}^{-1}\mathbf{f}\mathbf{f}^{\mathrm{T}}\mathbf{C}^{-1}}{1+s_\alpha^2\mathbf{f}^{\mathrm{T}}\mathbf{C}^{-1}\mathbf{f}}\right)\mathbf{f}\\ &-\mu_\alpha\sum_{j=1}^{K}\mathbf{f}^{\mathrm{T}}\left(\mathbf{C}^{-1}-\frac{s_\alpha^2\mathbf{C}^{-1}\mathbf{f}\mathbf{f}^{\mathrm{T}}\mathbf{C}^{-1}}{1+s_\alpha^2\mathbf{f}^{\mathrm{T}}\mathbf{C}^{-1}\mathbf{f}}\right)\mathbf{f}=0\end{aligned} \tag{36}$$

$$\begin{aligned}\frac{\partial l(\boldsymbol{\eta}|\mathbf{Y})}{\partial s_\alpha^2} = &-K\mathbf{f}^{\mathrm{T}}\mathbf{C}^{-1}\mathbf{f}\left(1+s_\alpha^2\mathbf{f}^{\mathrm{T}}\mathbf{C}^{-1}\mathbf{f}\right)\\ &+\sum_{j=1}^{K}\left(\mathbf{f}^{\mathrm{T}}\mathbf{C}^{-1}\mathbf{Y}_j\right)^2+\frac{\left(\sum_{j=1}^{K}\mathbf{Y}_j{}^{\mathrm{T}}\mathbf{C}^{-1}\mathbf{f}\right)^2}{K}=0.\end{aligned} \tag{37}$$

By solving (36) and (37), we obtain the MLE estimators of μ_α and s_α^2 as in (15) and (16), respectively.

B. Details of $W_1 - W_6$

The results of $W_1 - W_6$ in (19) and (20) are derived as follows:

$$\begin{aligned}W_1 = &\frac{\sum_{j=1}^{K}\mathbf{Y}_j^{\mathrm{T}}\mathbf{C}^{-1}\frac{\partial\mathbf{C}}{\partial\sigma^2}\mathbf{C}^{-1}\mathbf{f}}{K\mathbf{f}^{\mathrm{T}}\mathbf{C}^{-1}\mathbf{f}}\\ &-\frac{K\mathbf{f}^{\mathrm{T}}\mathbf{C}^{-1}\frac{\partial\mathbf{C}}{\partial\sigma^2}\mathbf{C}^{-1}\mathbf{f}\sum_{j=1}^{K}\mathbf{Y}_j^{\mathrm{T}}\mathbf{C}^{-1}\mathbf{f}}{\left(K\mathbf{f}^{\mathrm{T}}\mathbf{C}^{-1}\mathbf{f}\right)^2}\end{aligned} \tag{38}$$

$$\begin{aligned}W_2 = &\frac{\sum_{j=1}^{K}\mathbf{Y}_j^{\mathrm{T}}\mathbf{C}^{-1}\frac{\partial\mathbf{C}}{\partial H}\mathbf{C}^{-1}\mathbf{f}}{K\mathbf{f}^{\mathrm{T}}\mathbf{C}^{-1}\mathbf{f}}\\ &-\frac{K\mathbf{f}^{\mathrm{T}}\mathbf{C}^{-1}\frac{\partial\mathbf{C}}{\partial H}\mathbf{C}^{-1}\mathbf{f}\sum_{j=1}^{K}\mathbf{Y}_j^{\mathrm{T}}\mathbf{C}^{-1}\mathbf{f}}{\left(K\mathbf{f}^{\mathrm{T}}\mathbf{C}^{-1}\mathbf{f}\right)^2}\end{aligned} \tag{39}$$

$$W_3 = \frac{\sum_{j=1}^{K}\mathbf{Y}_j^{\mathrm{T}}\mathbf{C}^{-1}\mathbf{C}^{-1}\mathbf{f}}{K\mathbf{f}^{\mathrm{T}}\mathbf{C}^{-1}\mathbf{f}} - \frac{K\mathbf{f}^{\mathrm{T}}\mathbf{C}^{-1}\mathbf{C}^{-1}\mathbf{f}\sum_{j=1}^{K}\mathbf{Y}_j^{\mathrm{T}}\mathbf{C}^{-1}\mathbf{f}}{\left(K\mathbf{f}^{\mathrm{T}}\mathbf{C}^{-1}\mathbf{f}\right)^2} \tag{40}$$

$$\begin{aligned}W_4 = &\frac{\mathbf{f}^{\mathrm{T}}\mathbf{C}^{-1}\frac{\partial\mathbf{C}}{\partial\sigma^2}\mathbf{C}^{-1}\mathbf{f}}{\left(\mathbf{f}^{\mathrm{T}}\mathbf{C}^{-1}\mathbf{f}\right)^2}+\frac{\sum_{j=1}^{K}2\mathbf{Y}_j{}^{\mathrm{T}}\mathbf{C}^{-1}\mathbf{f}\mathbf{Y}_j{}^{\mathrm{T}}\mathbf{C}^{-1}\frac{\partial\mathbf{C}}{\partial\sigma^2}\mathbf{C}^{-1}\mathbf{f}}{K\left(\mathbf{f}^{\mathrm{T}}\mathbf{C}^{-1}\mathbf{f}\right)^2}\\ &-\frac{2K\mathbf{f}^{\mathrm{T}}\mathbf{C}^{-1}\mathbf{f}\mathbf{f}^{\mathrm{T}}\mathbf{C}^{-1}\frac{\partial\mathbf{C}}{\partial\sigma^2}\mathbf{C}^{-1}\mathbf{f}\sum_{j=1}^{K}\left(\mathbf{Y}_j{}^{\mathrm{T}}\mathbf{C}^{-1}\mathbf{f}\right)^2}{K^2\left(\mathbf{f}^{\mathrm{T}}\mathbf{C}^{-1}\mathbf{f}\right)^4}\\ &-\frac{2\left(\sum_{j=1}^{K}\mathbf{Y}_j^{\mathrm{T}}\mathbf{C}^{-1}\mathbf{f}\right)\left(\sum_{j=1}^{K}\mathbf{Y}_j^{\mathrm{T}}\mathbf{C}^{-1}\frac{\partial\mathbf{C}}{\partial\sigma^2}\mathbf{C}^{-1}\mathbf{f}\right)}{\left(K\mathbf{f}^{\mathrm{T}}\mathbf{C}^{-1}\mathbf{f}\right)^2}\\ &+\frac{2K^2\mathbf{f}^{\mathrm{T}}\mathbf{C}^{-1}\mathbf{f}\mathbf{f}^{\mathrm{T}}\mathbf{C}^{-1}\frac{\partial\mathbf{C}}{\partial\sigma^2}\mathbf{C}^{-1}\mathbf{f}\left(\sum_{j=1}^{K}\mathbf{Y}_j^{\mathrm{T}}\mathbf{C}^{-1}\mathbf{f}\right)^2}{\left(K\mathbf{f}^{\mathrm{T}}\mathbf{C}^{-1}\mathbf{f}\right)^4}\end{aligned} \tag{41}$$

$$\begin{aligned}W_5 = &\frac{\mathbf{f}^{\mathrm{T}}\mathbf{C}^{-1}\frac{\partial\mathbf{C}}{\partial H}\mathbf{C}^{-1}\mathbf{f}}{\left(\mathbf{f}^{\mathrm{T}}\mathbf{C}^{-1}\mathbf{f}\right)^2}+\frac{\sum_{j=1}^{K}2\mathbf{Y}_j{}^{\mathrm{T}}\mathbf{C}^{-1}\mathbf{f}\mathbf{Y}_j{}^{\mathrm{T}}\mathbf{C}^{-1}\frac{\partial\mathbf{C}}{\partial H}\mathbf{C}^{-1}\mathbf{f}}{K\left(\mathbf{f}^{\mathrm{T}}\mathbf{C}^{-1}\mathbf{f}\right)^2}\\ &-\frac{2K\mathbf{f}^{\mathrm{T}}\mathbf{C}^{-1}\mathbf{f}\mathbf{f}^{\mathrm{T}}\mathbf{C}^{-1}\frac{\partial\mathbf{C}}{\partial H}\mathbf{C}^{-1}\mathbf{f}\sum_{j=1}^{K}\left(\mathbf{Y}_j{}^{\mathrm{T}}\mathbf{C}^{-1}\mathbf{f}\right)^2}{K^2\left(\mathbf{f}^{\mathrm{T}}\mathbf{C}^{-1}\mathbf{f}\right)^4}\\ &-\frac{2\left(\sum_{j=1}^{K}\mathbf{Y}_j^{\mathrm{T}}\mathbf{C}^{-1}\mathbf{f}\right)\left(\sum_{j=1}^{K}\mathbf{Y}_j^{\mathrm{T}}\mathbf{C}^{-1}\frac{\partial\mathbf{C}}{\partial H}\mathbf{C}^{-1}\mathbf{f}\right)}{\left(K\mathbf{f}^{\mathrm{T}}\mathbf{C}^{-1}\mathbf{f}\right)^2}\\ &+\frac{2K^2\mathbf{f}^{\mathrm{T}}\mathbf{C}^{-1}\mathbf{f}\mathbf{f}^{\mathrm{T}}\mathbf{C}^{-1}\frac{\partial\mathbf{C}}{\partial H}\mathbf{C}^{-1}\mathbf{f}\left(\sum_{j=1}^{K}\mathbf{Y}_j^{\mathrm{T}}\mathbf{C}^{-1}\mathbf{f}\right)^2}{\left(K\mathbf{f}^{\mathrm{T}}\mathbf{C}^{-1}\mathbf{f}\right)^4}\end{aligned} \tag{42}$$

$$\begin{aligned}W_6 = &\frac{\mathbf{f}^{\mathrm{T}}\mathbf{C}^{-1}\mathbf{C}^{-1}\mathbf{f}}{\left(\mathbf{f}^{\mathrm{T}}\mathbf{C}^{-1}\mathbf{f}\right)^2}+\frac{\sum_{j=1}^{K}2\mathbf{Y}_j{}^{\mathrm{T}}\mathbf{C}^{-1}\mathbf{f}\mathbf{Y}_j{}^{\mathrm{T}}\mathbf{C}^{-1}\mathbf{C}^{-1}\mathbf{f}}{K\left(\mathbf{f}^{\mathrm{T}}\mathbf{C}^{-1}\mathbf{f}\right)^2}\\ &-\frac{2K\mathbf{f}^{\mathrm{T}}\mathbf{C}^{-1}\mathbf{f}\mathbf{f}^{\mathrm{T}}\mathbf{C}^{-1}\mathbf{C}^{-1}\mathbf{f}\sum_{j=1}^{K}\left(\mathbf{Y}_j{}^{\mathrm{T}}\mathbf{C}^{-1}\mathbf{f}\right)^2}{K^2\left(\mathbf{f}^{\mathrm{T}}\mathbf{C}^{-1}\mathbf{f}\right)^4}\\ &-\frac{2\left(\sum_{j=1}^{K}\mathbf{Y}_j^{\mathrm{T}}\mathbf{C}^{-1}\mathbf{f}\right)\left(\sum_{j=1}^{K}\mathbf{Y}_j^{\mathrm{T}}\mathbf{C}^{-1}\mathbf{C}^{-1}\mathbf{f}\right)}{\left(K\mathbf{f}^{\mathrm{T}}\mathbf{C}^{-1}\mathbf{f}\right)^2}\\ &+\frac{2K^2\mathbf{f}^{\mathrm{T}}\mathbf{C}^{-1}\mathbf{f}\mathbf{f}^{\mathrm{T}}\mathbf{C}^{-1}\mathbf{C}^{-1}\mathbf{f}\left(\sum_{j=1}^{K}\mathbf{Y}_j^{\mathrm{T}}\mathbf{C}^{-1}\mathbf{f}\right)^2}{\left(K\mathbf{f}^{\mathrm{T}}\mathbf{C}^{-1}\mathbf{f}\right)^4}\end{aligned} \tag{43}$$

and the (u,v)th entry of matrices $\frac{\partial\mathbf{C}}{\partial\sigma^2}$ and $\frac{\partial\mathbf{C}}{\partial H}$ is calculated, respectively, by

$$\left(\frac{\partial\mathbf{C}}{\partial\sigma^2}\right)_{uv} = \frac{1}{2}\left(t_u{}^{2H}+t_v{}^{2H}-|t_u-t_v|^{2H}\right) \tag{44}$$

$$\left(\frac{\partial\mathbf{C}}{\partial H}\right)_{uv} = \begin{cases}\sigma^2\left(t_u{}^{2H}\ln(t_u)+t_v{}^{2H}\ln(t_v)\right); & \text{for } u=v\\ \sigma^2\left(t_u{}^{2H}\ln(t_u)+t_v{}^{2H}\ln(t_v)\right.\\ \left.-|t_u-t_v|^{2H}\ln|t_u-t_v|\right); & \text{for } u\neq v\end{cases}. \tag{45}$$

TABLE XII
POINT ESTIMATES AND STANDARD ERRORS OF P_3 PARAMETERS UNDER THREE LEVELS OF MEASUREMENT ERRORS

$P_3\,(d^2=0.1)$		
Parameter	Point Estimate	Standard Error
H	0.880	0.0372
σ^2	0.406	0.0787
d^2	0.103	0.00739
μ_α	5.24	0.0304
s_α^2	0.532	0.223
β	0.684	0.0159
$P_3\,(d^2=0.5)$		
Parameter	Point Estimate	Standard Error
H	0.841	0.0531
σ^2	0.468	0.0771
d^2	0.482	0.0297
μ_α	5.09	0.0688
s_α^2	1.09	0.181
β	0.703	0.0171
$P_3\,(d^2=1.0)$		
Parameter	Point Estimate	Standard Error
H	0.839	0.0562
σ^2	0.527	0.0832
d^2	1.03	0.0573
μ_α	5.41	0.102
s_α^2	0.585	0.192
β	0.683	0.0213

C. Effect of Signal-to-Noise Ratio

A simulation study is conducted to verify the proposed model under various amplitude levels of measurement errors. Specifically, based on model P_3, degradation paths are generated under three higher levels of measurement errors, i.e., $d^2 = 0.1, 0.5,$ and 1.0, whereas all other parameters are the same as described in Section IV-B. Using the MLE approach, the parameter estimation results are obtained and summarized in Table XII.

From Table XII, it can be seen that the point estimates of model parameters are all close to the specified values, which demonstrates the robustness of the proposed model under various levels of signal-to-noise ratio. To further verify the proposed model, reliability analyses are also conducted under a failure threshold of $y_{th} = 100$. The PDFs of lifetime along with the true lifetime histogram are illustrated in Fig. 10. It can be seen that the predicted lifetime distributions under the three levels of measurement errors are all close to the true lifetime distribution. This further demonstrates the robustness of the proposed model under various levels of signal-to-noise ratio.

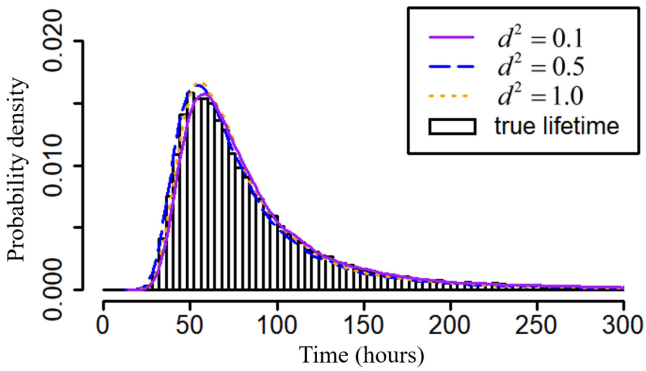

Fig. 10. PDFs of the predicted lifetime using P_3 when $d^2 = 0.1, 0.5,$ and 1.0.

ACKNOWLEDGMENT

The authors would like to thank the Associate Editor and three Referees for providing constructive comments that helped improve this article.

REFERENCES

[1] Z. Ye, Y. Wang, K. Tsui, and M. Pecht, "Degradation data analysis using wiener processes with measurement errors," *IEEE Trans. Rel.*, vol. 62, no. 4, pp. 772–780, Dec. 2013.
[2] Z. Xu, Y. Hong, and R. Jin, "Nonlinear general path models for degradation data with dynamic covariates," *Appl. Stochastic Models Bus. Ind.*, vol. 32, no. 2, pp. 153–167, 2016.
[3] X. Fang, N. Z. Gebraeel, and K. Paynabar, "Scalable prognostic models for large-scale condition monitoring applications," *IISE Trans.*, vol. 49, no. 7, pp. 698–710, 2017.
[4] X. Xi, M. Chen, and D. Zhou, "Remaining useful life prediction for degradation processes with memory effects," *IEEE Trans. Rel.*, vol. 66, no. 3, pp. 751–760, Sep. 2017.
[5] H. Zhang, M. Chen, X. Xi, and D. Zhou, "Remaining useful life prediction for degradation processes with long-range dependence," *IEEE Trans. Rel.*, vol. 66, no. 4, pp. 1368–1379, Dec. 2017.
[6] H. Zhang, Z. Mo, J. Wang, and Q. Miao, "Nonlinear-drifted fractional brownian motion with multiple hidden state variables for remaining useful life prediction of lithium-ion batteries," *IEEE Trans. Rel.*, vol. 69, no. 2, pp. 768–780, Jun. 2020.
[7] W. Si, Y. Shao, and W. Wei, "Accelerated degradation testing with long-term memory effects," *IEEE Trans. Rel.*, vol. 69, no. 4, pp. 1254–1266, Dec. 2020.
[8] T. Sottinen, "Fractional brownian motion, random walks and binary market models," *Finance Stochastics*, vol. 5, no. 3, pp. 343–355, 2001.
[9] A. Montanari, "Long-range dependence in hydrology," in *Theory and Applications of Long-Range Dependence*. Cambridge, MA, USA: Birkhäuser, 2003, pp. 461–472.
[10] K. Burnecki, E. Kepten, J. Janczura, I. Bronshtein, Y. Garini, and A. Weron, "Universal algorithm for identification of fractional brownian motion. A case of telomere subdiffusion," *Biophys. J.*, vol. 103, no. 9, pp. 1839–1847, 2012.
[11] H. Zhang, D. Zhou, M. Chen, and X. Xi, "Predicting remaining useful life based on a generalized degradation with fractional brownian motion," *Mech. Syst. Signal Process.*, vol. 115, pp. 736–752, 2019.
[12] W. Song, X. Chen, C. Cattani, and E. Zio, "Multifractional brownian motion and quantum-behaved partial swarm optimization for bearing degradation forecasting," *Complexity*, vol. 2020, 2020, Art. no. 8543131.
[13] H. Wang, W. Song, E. Zio, A. Kudreyko, and Y. Zhang, "Remaining useful life prediction for Lithium-ion batteries using fractional brownian motion and fruit-fly optimization algorithm," *Measurement*, vol. 161, 2020, Art. no. 107904.
[14] F. L. Schmidt and J. E. Hunter, "Measurement error in psychological research: Lessons from 26 research scenarios," *Psychol. Methods*, vol. 1, no. 2, pp. 199–223, 1996.

[15] D. M. Rocke and B. Durbin, "A model for measurement error for gene expression arrays," *J. Comput. Biol.*, vol. 8, no. 6, pp. 557–569, 2001.
[16] J. A. Hutcheon, A. Chiolero, and J. A. Hanley, "Random measurement error and regression dilution bias," *Brit. Med. J.*, vol. 340, 2010, Art. no. c2289.
[17] J. Miller and J. C. Miller, *Statistics and Chemometrics for Analytical Chemistry*, 6th ed. London, U.K.: Pearson, 2010.
[18] D. Liu and S. Wang, "Reliability estimation from lifetime testing data and degradation testing data with measurement error based on evidential variable and wiener process," *Rel. Eng. Syst. Saf.*, vol. 205, 2021, Art. no. 107231.
[19] C. J. Lu and W. Meeker, "Using degradation measures to estimate a time-to-failure distribution," *Technometrics*, vol. 35, no. 2, pp. 161–174, 1993.
[20] W. Si, Q. Yang, X. Wu, and Y. Chen, "Reliability analysis considering dynamic material local deformation," *J. Qual. Technol.*, vol. 50, no. 2, pp. 183–197, 2018.
[21] W. Q. Meeker, L. A. Escobar, and C. J. Lu, "Accelerated degradation tests: Modeling and analysis," *Technometrics*, vol. 40, no. 2, pp. 89–99, 1998.
[22] L. Lu, B. Wang, Y. Hong, and Z. Ye, "General path models for degradation data with multiple characteristics and covariates," *Technometrics*, vol. 63, pp. 354–369, 2020, doi: 10.1080/00401706.2020.1796814.
[23] M. H. Ling, K. L. Tsui, and N. Balakrishnan, "Accelerated degradation analysis for the quality of a system based on the gamma process," *IEEE Trans. Rel.*, vol. 64, no. 1, pp. 463–472, Mar. 2015.
[24] Z. Ye, M. Xie, L. Tang, and N. Chen, "Semiparametric estimation of gamma processes for deteriorating products," *Technometrics*, vol. 56, no. 4, pp. 504–513, 2014.
[25] X. Wang and D. Xu, "An inverse gaussian process model for degradation data," *Technometrics*, vol. 52, no. 2, pp. 188–197, 2010.
[26] Z. Ye and N. Chen, "The inverse Gaussian process as a degradation model," *Technometrics*, vol. 56, no. 3, pp. 302–311, 2014.
[27] Z. Ye, N. Chen, and Y. Shen, "A new class of Wiener process models for degradation analysis," *Rel. Eng. Syst. Saf.*, vol. 139, pp. 58–67, 2015.
[28] Z. Zhang, X. Si, C. Hu, and Y. Lei, "Degradation data analysis and remaining useful life estimation: A review on Wiener-process-based methods," *Eur. J. Oper. Res.*, vol. 271, no. 3, pp. 775–796, 2018.
[29] G. Whitmore, "Estimating degradation by a Wiener diffusion process subject to measurement error," *Lifetime Data Anal.*, vol. 1, no. 3, pp. 307–319, 1995.
[30] Y. Zhou and M. Huang, "Lithium-ion batteries remaining useful life prediction based on a mixture of empirical mode decomposition and ARIMA model," *Microelectron. Rel.*, vol. 65, pp. 265–273, 2016.
[31] M. Kim, C. Song, and K. Liu, "A generic health index approach for multisensor degradation modeling and sensor selection," *IEEE Trans. Autom. Sci. Eng.*, vol. 16, no. 3, pp. 1426–1437, Jul. 2019.
[32] J. Zhu, N. Chen, and W. Peng, "Estimation of bearing remaining useful life based on multiscale convolutional neural network," *IEEE Trans. Ind. Electron.*, vol. 66, no. 4, pp. 3208–3216, Apr. 2019.
[33] F. Wang, J. Du, Y. Zhao, T. Tang, and J. Shi, "A deep learning based data fusion method for degradation modeling and prognostics," *IEEE Trans. Rel.*, vol. 70, no. 2, pp. 775–789, Jun. 2021.
[34] B. B. Mandelbrot and J. W. Van Ness, "Fractional brownian motions, fractional noises and applications," *SIAM Rev.*, vol. 10, no. 4, pp. 422–437, 1968.
[35] H. Zhang, D. Zhou, M. Chen, and J. Shang, "FBM-based remaining useful life prediction for degradation processes with long-range dependence and multiple modes," *IEEE Trans. Rel.*, vol. 68, no. 3, pp. 1021–1033, Sep. 2019.
[36] X. Xi, D. Zhou, and M. Chen, "Prognostics of non-Markovian degradation processes with fractal property and measurement uncertainty," in *Proc. 3rd Int. Conf. Syst. Rel. Saf.*, Barcelona, Spain, 2018, pp. 235–243.
[37] E. Alòs and D. Nualart, "Stochastic integration with respect to the fractional Brownian motion," *Stochastics Stochastics Rep.*, vol. 75, no. 3, pp. 129–152, 2003.
[38] G. Casella and R. L. Berger, *Statistical Inference*. Pacific Grove, CA, USA: Johns Hopkins Univ., 2002.
[39] V. Schmidt and S. Geometry, *Spatial Statistics and Random Fields*. Berlin, Germany: Springer, 2014.
[40] J. R. Hosking, "Modeling persistence in hydrological time series using fractional differencing," *Water Resour. Res.*, vol. 20, no. 12, pp. 1898–1908, 1984.
[41] S. Asmussen, *Stochastic Simulation With a View Towards Stochastic Processes*. Aarhus, Denmark: Centre Math. Phys. Stochastics, Univ. Aarhus, 1998.
[42] A. B. Dieker and M. Mandjes, "On spectral simulation of fractional Brownian motion," *Probab. Eng. Inf. Sci.*, vol. 17, no. 3, pp. 417–434, 2003.
[43] H. Guo and H. Liao, "Practical approaches for reliability evaluation using degradation data," in *Proc. Annu. Rel. Maintainability Symp.*, Palm Harbor, FL, USA, 2015, vol. 7.
[44] C. Birkl and D. Howey, "Oxford Battery Degradation Dataset 1-Long term battery ageing tests of 8 Kokam (SLPB533459H4) 740 mAh lithium-ion pouch cells," Univ. Oxford, Oxford, U.K., 2017, doi: 10.5287/bodleian:KO2kdmYGg.
[45] C. Pozrikidis, *An Introduction to Grids, Graphs, and Networks*. London, U.K.: Oxford Univ. Press, 2014.
[46] W. H. Press, S. A. Teukolsky, W. T. Vetterling, and B. P. Flannery, *Numerical Recipes: The Art of Scientific Computing*, 3rd ed. Cambridge, U.K.: Cambridge Univ. Press, 2007.

Yunfei Shao received the B.S. degree in theoretical and applied mechanics from the University of Science and Technology of China, Hefei, China, in 2016. He is currently working toward the Ph.D. degree in industrial engineering with the Department of Industrial, Systems, and Manufacturing Engineering, Wichita State University, Wichita, KS, USA.

His research interests include the development of statistical and data mining methods in reliability engineering and maintenance planning.

Wujun Si received the B.Eng. degree in mechanical engineering from the University of Science and Technology of China, Hefei, China, in 2013, and the Ph.D. degree in industrial engineering from Wayne State University, Detroit, MI, USA, in 2018.

He is currently an Assistant Professor with the Department of Industrial, Systems, and Manufacturing Engineering, Wichita State University, Wichita, KS, USA. His work has been published in *Technometrics*, *Journal of Quality Technology*, *IISE Transactions*, *Computers & Operations Research*, and IEEE TRANSACTIONS ON RELIABILITY, among others. His research interests include engineering statistics and artificial intelligence for reliability analysis and quality control of complex systems.